Nonlinear Dyn (2012) 67:1969–1984
DOI 10.1007/s11071-011-0122-3

ORIGINAL PAPER

Bifurcation and chaos of a cable–beam coupled system under simultaneous internal and external resonances

M.H. Wei · Y.Q. Xiao · H.T. Liu

Received: 12 January 2011 / Accepted: 2 June 2011 / Published online: 9 July 2011

Abstract The bifurcation and chaos of a cable–beam coupled system under simultaneous internal and external resonances are investigated. The combined effects of the nonlinear term due to the cable's geometric and coupled behavior between the modes of the beam and the cable are considered. The nonlinear partial-differential equations are derived by the Hamiltonian principle. The Galerkin method is applied to truncate the governing equation into a set of ordinary differential equations. The bifurcation diagrams in three separate loading cases, namely, excitation acting on the cable, on the beam and simultaneously on the beam and cable, are analyzed with changing forcing amplitude. Based on careful numerical simulations, bifurcations and possible chaotic motions are represented to reveal the combined effects of nonlinearities on the dynamics of the beam and the cable when they act as an overall structure.

Keywords Cable–beam coupled system · Internal resonant · External resonant · Bifurcation · Chaos

1 Introduction

Many fields of engineering, including tower cranes, stayed bridges, guyed masts, and suspended roofs, can be reduced to a cable–beam coupled system model. Investigations into the nonlinear dynamics of these structures have conventionally focused on the substructure, i.e., the cable or the beam. However, this cable–beam coupled system consists of a beam and a cable with each fixed at one end and attached at the other end. As a result, nonlinearities in these dynamical systems are formed as a result of the cable's geometry and the coupled behavior between the modes of the beam and the cable. On the other hand, if the beam and the cable act as an overall structure in these fields, there are some new mechanisms, such as internal resonance and external resonance, as well as a combination of the two resonances. Therefore, the bifurcation and chaos dynamics of these structures must be studied in terms of an overall structure.

Since a single beam and cable are widely used in engineering, a great deal of literatures on their bifurcation and chaos has been published that examines a variety of phenomena under various conditions [1–6]. However, in order to comprehend the bifurcation and chaos of the cable–beam coupled system, additional knowledge regarding the coupled behavior that occurs due to internal resonance between the modes of the beam and the cable must be required. From the viewpoint of modal coupling, Mamandi [7] investigated the nonlinear dynamic response of an inclined Timoshenko beam coupled with a traveling mass that has variable velocity. Kenfack [8] investigated the bifurcation structure of coupled periodically driven double-well Duffing oscillators, and fur-

M.H. Wei · Y.Q. Xiao (✉) · H.T. Liu
Shenzhen Graduate School, Harbin Institute of Technology, Shenzhen 518055, China
e-mail: xiaoyq@hit.edu.cn

ther analyzed by Musielak [9] with multiple degrees of freedom. Cao and Zhang [10, 11] investigated the global bifurcation and chaotic dynamics of a string-beam coupled system through analytical study and numerical simulation. Nevertheless, little study has been devoted to the analysis of the bifurcation and chaos of a cable–beam coupled system.

In fact, there are many internal resonance forms between the modes of a beam and a cable when they act as an overall structure, such as two-to-one, one-to-one, one-to-two, etc. However, the last have occurred very often in constructions over the past decade [12–14]. Therefore, this study focuses on the bifurcation and chaos of a cable–beam coupled system in the case of one-to-two internal resonance, taking into consideration the external resonance to the beam or the cable due to loading case changing. The combined effects of nonlinear terms due to the cable's geometric and coupled behavior between the modes of the beam and the cable are considered. The governing equations of the cable–beam coupled system due to vertical excitation acting on the beam and the cable are derived by the Hamiltonian principle. The Galerkin method is applied to truncate the governing equations into a set of nonlinear ordinary differential equations. In numeral investigations, when the bifurcation and chaos of the cable–beam coupled system in the three loading cases are investigated for the combination of internal and external resonances, the harmonic forcing magnitude is chosen as a controlling parameter. It is demonstrated that rich dynamics occur in these cases. A corresponding comparison is made between these cases and the identified differences are briefly discussed and some possible explanations put forward.

2 Equations of motion

To conveniently analyze the dynamic characteristics of the cable–beam coupled system, a model consisting of a beam and cable, each fixed at one end and attached at the other, as shown in Fig. 1, is considered. The beam is modeled as an Euler–Bernoulli beam, the cable is modeled neglecting the bending, torsional and shear rigidities, and the cable sag to span ratio is very small ($d/l_c < 0.1$). In addition, we assume that the beam and cable under consideration are homogeneous and only oscillate transversely on the plane.

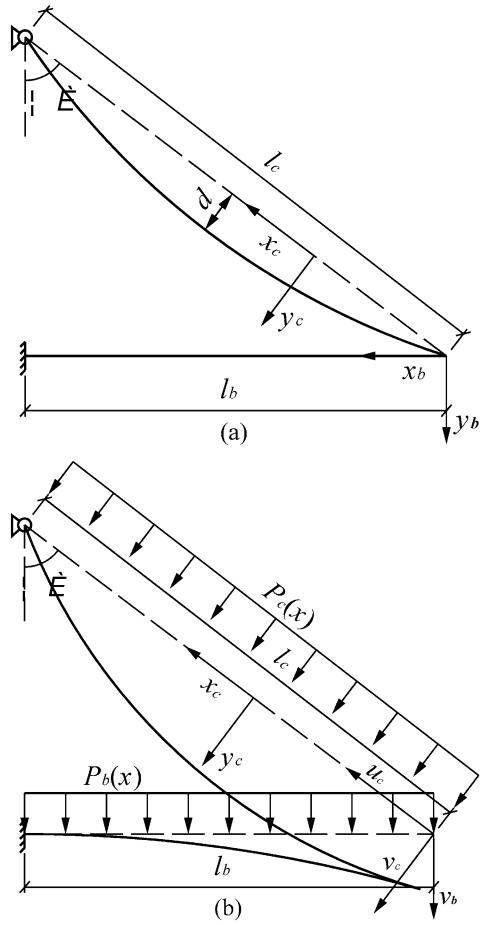

Fig. 1 Sketch of cable–beam structure: (**a**) static model; (**b**) dynamic model

Based on the above assumptions, the governing equations of motion for the cable–beam coupled system are obtained by using the extended Hamilton principle, which states that

$$\int_{t_1}^{t_2} (\delta T - \delta V - \delta W)\, dt = 0 \tag{1}$$

where δT, δV, and δW are the kinetic energy, potential energy and work done by gravity, respectively, and are given by:

$$T_b = \frac{1}{2}\int_0^{l_b} m_b \dot{v}_b^2\, dx_b = 0 \tag{2a}$$

$$T_c = \frac{1}{2}\int_0^{l_c} m_c\left(\dot{u}_c^2 + \dot{v}_c^2\right) ds_c = 0 \tag{2b}$$

$$V_b = \frac{1}{2}\int_0^{l_b} N(v_b')^2\,dx_b + \frac{1}{2}\int_0^{l_b} E_b I_b (v_b'')^2\,dx_b \quad (3a)$$

$$V_c = \frac{1}{2}\int_0^{l_c} E_c A_c \varepsilon_c^2\,ds_0 + \int_0^{l_c} H\frac{ds_0}{dx_c}\varepsilon_c\,ds_0 \quad (3b)$$

$$W_c = \int_0^{l_c} m_c g\big(u_c\cos(\theta) + v_c\sin(\theta)\big)\,ds_0 \quad (4)$$

where the symbols m_b and m_c are the mass per unit length of the beam and cable, respectively; l_b and l_c are the length of the beam and cable, respectively; E_bI_b and E_cA_c are the bending stiffness of the beam and axial stiffness of the cable, respectively, and E_b, E_c are Young's modulus of the beam and cable materials, respectively; I_b, A_c are the moment of area of the beam and the cross-sectional area of the cable, respectively; N is the axial compressive load; H is the initial tension of the cable; v_b is the beam displacement at location x_b and time t; and u_c, v_c are the longitudinal and transversal displacements of the cable at location x_c and time t, respectively. The overdot indicates differentiation with respect to time t; the prime indicates differentiation with respect to the coordinate x.

Since the transverse wave speed is much lower than the longitudinal wave speed for the cables, the stretches of the cable are assumed to have a quasi-static manner, $y_c = 4d[x_c/l_c - (x_c/l_c)^2]$. On the other hand, assuming small sag to span ratio, then $ds_0 = dx_c$. The expression of the elongation for the cable has the following form:

$$\varepsilon_c = \frac{ds - ds_0}{ds_0} = \frac{du_c}{ds_0}\frac{dx_c}{ds_0} + \frac{dy_c}{ds_0}\frac{dv_c}{ds_0} + \frac{1}{2}\left(\frac{dv_c}{ds_0}\right)^2 \quad (5)$$

in which

$$ds_0^2 = dx_c^2 + dy_c^2 \quad (6a)$$

$$ds^2 = (dx_c + du_c)^2 + (dy_c + dv_c)^2 \quad (6b)$$

On substituting (2a)–(6b) into Hamilton's energy (1) and on integrating by parts, the equations of motion are derived as:

$$m_b\ddot{v}_b + E_bI_bv_b'''' + Nv_b'' = 0 \quad (7a)$$

$$m_c\ddot{u}_c - \left[E_cA_c\left(u_c' + y_c'v_c' + \frac{1}{2}v_c'^2\right)\right]' = 0 \quad (7b)$$

$$m_c\ddot{v}_c - \Big[Hv_c' + E_cA_c(y_c' + v_c') \times \left(u_c' + y_c'v_c' + \frac{1}{2}v_c'^2\right)\Big]' = 0 \quad (7c)$$

The associated geometric boundary conditions of the beam and cable are written as:

$$\begin{aligned} &u_c(0,t)\sin(\theta) + v_c(0,t)\cos(\theta) = 0,\\ &u_c(l_c,t) = 0, \qquad v_c(l_c,t) = 0,\\ &v_c(0,t)\sin(\theta) - u_c(0,t)\cos(\theta) = v_b(0,t),\\ &v_b(l_b,t) = 0, \qquad v_b(l_b,t)' = 0 \end{aligned} \quad (8)$$

The relevant mechanical boundary conditions are written as [15]:

$$v_b(0,t)'' = 0, \qquad E_bI_bv_b(0,t)''' + kv_b(0,t) = 0 \quad (9)$$

where $k = E_cA_c\cos(\theta)^2/l_c$ is the stiffness of the cable supporting the beam.

Neglecting the axial inertia in the cable, the elongation of the cable can be derived from (7b) as

$$e(t,x_c) = u_c' + y_c'v_c' + \frac{1}{2}v_c'^2 \quad (10)$$

By manipulating (10), (12a) and (12b), the following uniform dynamic elongation can be obtained:

$$e(t) = \frac{1}{l_c}v_b(0,t)\cos(\theta) + \frac{1}{l_c}\int_0^{l_c}\left(y_c'v_c' + \frac{1}{2}v_c'^2\right)dx_c \quad (11)$$

$$m_b\ddot{v}_b^2 + \xi_b\dot{v}_b + E_bI_bv_b'''' + Nv_b'' = p_b\cos(\Omega_1 t) \quad (12a)$$

$$m_c\ddot{v}_c + \xi_c\dot{v}_c - \big[Hv_c' + E_cA_ce(t)(y_c' + v_c')\big]' = p_c\cos(\Omega_2 t) \quad (12b)$$

where ξ_b and ξ_c are the damping coefficients of the beam and cable, respectively; Ω_1, Ω_2, and p_b, p_c are the frequency and forcing amplitude on the beam and cable, respectively; and N is the axial compressive load and is given by:

$$N = \big(H + E_cA_ce(t)\big)\sin(\theta) \quad (13)$$

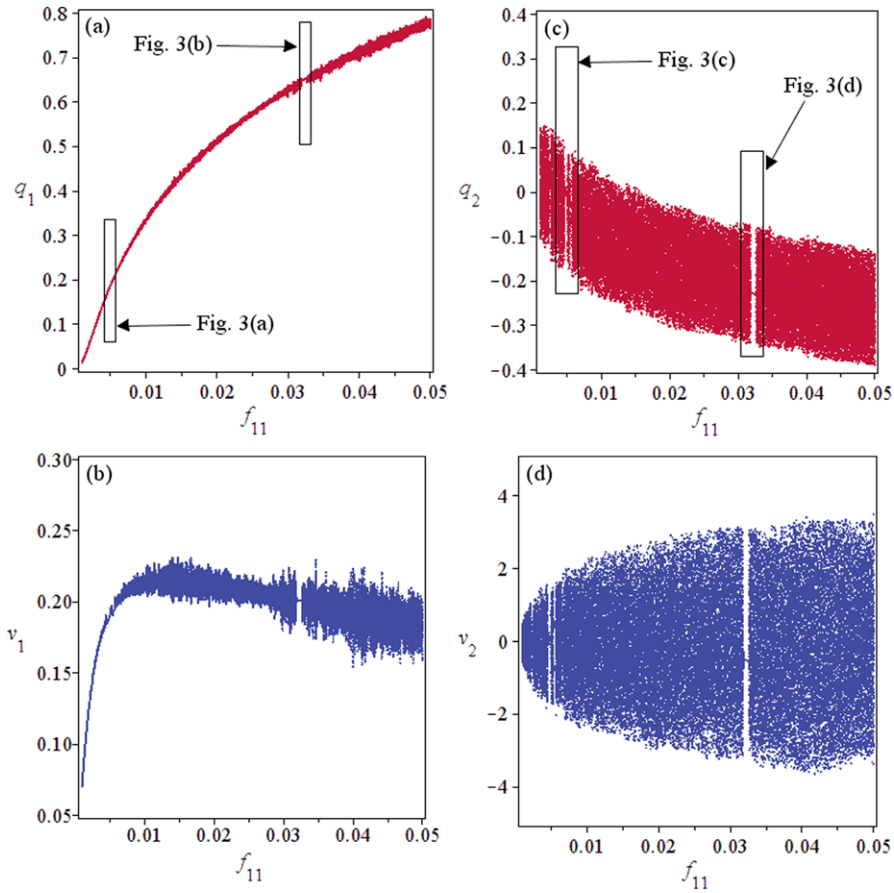

Fig. 2 Bifurcation diagrams for the primary resonance to the beam ($\omega_1 : \Omega_1 = 1:1$) and auto parametric resonance to the cable ($\omega_2 : \Omega_1 = 2:1$) when the excitation directly acting on the beam: (**a**) the beam's modal amplitude; (**b**) the beam's modal velocity; (**c**) the cable's modal amplitude; (**d**) the cable's modal velocity

For convenience, a set of new variables and parameters are defined as:

$$\overline{y} = \frac{y}{d}, \qquad \tau = \omega t, \qquad \overline{x_i} = \frac{x_i}{l_i}, \qquad \overline{v_i} = \frac{v_i}{l_i},$$
$$\overline{\xi_i} = \frac{\xi_i}{m_i \omega}, \qquad \overline{p_b} = \frac{p_b(x_b)}{m_b \omega^2 l_c}, \qquad \overline{\Omega} = \frac{\Omega}{\omega},$$
$$i = b, c \tag{14}$$
$$\rho = \frac{m_c}{m_b}, \qquad \mu = \frac{E_c A_c}{H}, \qquad \nu = \frac{d}{l_c},$$
$$\chi = \frac{E_b I_b}{l_b^2 E_c A_c}, \qquad \beta_c^2 = \omega^2 \frac{m_c l_c^2}{H}, \qquad \beta_b^4 = \omega^2 \frac{m_b l_b^4}{E_b I_b}$$

where ω is the natural frequency of the system in-plane. In the nondimensional form, (8)–(14) become:

$$\ddot{v}_1 + \xi_1 \dot{v}_1 + \frac{1}{\beta_b^4} v_1'''' + \frac{\rho}{\beta_c^2 \sin(\theta)} v_1'' + \frac{\rho \mu e}{\beta_c^2 \sin(\theta)} v_1'' = p_1 \cos(\Omega t) \tag{15a}$$

$$\ddot{v}_2 + \xi_2 \dot{v}_2 - \frac{1}{\beta_c^2}\left[v_2'' + \mu e (\nu y'' + v_2'')\right] = p_2 \cos(\Omega t) \tag{15b}$$

$$v_1(1,t) = 0, \qquad v_1(0,t)'' = 0,$$
$$v_2(1,t) = 0, \qquad v_2(1,t)' = 0 \tag{16a}$$

$$v_2(0,t) - v_1(0,t)\sin(\theta)^2 = 0, \ \chi v_1(0,t)''' + \cos(\theta)^2 \sin(\theta) v_1(0,t) = 0 \tag{16b}$$

where subscripts 1 and 2 denote subscripts b and c, respectively.

Based on research given by Cheng and Zu [16], the transverse displacements $v_1(x,t)$ and $v_2(x,t)$ are approximated by the vibration modes of the first order as follows:

$$v_1(x,t) = \varphi_1(x) q_1(t) \tag{17a}$$

$$v_2(x,t) = \varphi_2(x) q_2(t) + \varphi_1(x) q_1(t) \sin(\theta)^2 \tag{17b}$$

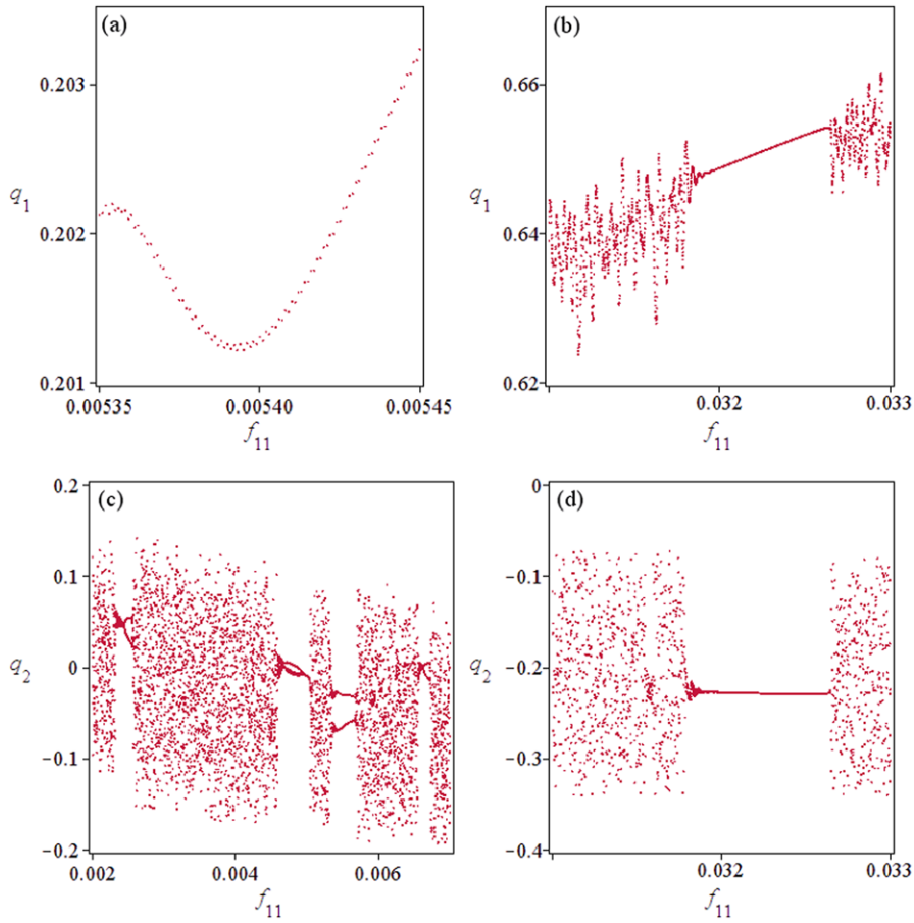

Fig. 3 Local magnification of Figs. 2(a) and 2(c)

where $\phi_1(x), \phi_2(x)$ are the mode shapes of the beam and the cable, respectively, and can be written as [17]:

$$\varphi_1(x) = A_1 \sin(\beta_c x) + A_2 \cos(\beta_c x) + A_3 \sinh(\beta_c x) + A_4 \cosh(\beta_c x) \tag{18a}$$

$$\varphi_2(x) = \frac{8\mu\nu e}{\beta_c^2}\left(1 - \tan\left(\frac{\beta_c}{2}\right)\sin(\beta_c x) - \cos(\beta_c x)\right) \tag{18b}$$

With these assumptions, the nonlinear governing equations of motion with two degrees-of-freedom for the cable–beam coupled system can be derived by substituting (17a), (17b) into (16a), (16b) and by implementing the Galerkin method. This yields the following set of equations:

$$\ddot{q}_1(t) + \xi_1\dot{q}_1(t) + a_1 q_1(t) + a_{12} q_1(t) q_2(t) + a_{122} q_1(t) q_2(t)^2 + a_{11} q_1(t)^2 + a_{112} q_1(t)^2 q_2(t) + a_{111} q_1(t)^3 = f_{11}\cos(\Omega_1 t) \tag{19a}$$

$$\ddot{q}_2(t) + \xi_2\dot{q}_2(t) + c_1\ddot{q}_1(t) + c_2\dot{q}_1(t) + b_2 q_2(t) + b_{12} q_1(t) q_2(t) + b_{112} q_1(t)^2 q_2(t) + b_{22} q_2(t)^2 + b_{112} q_1(t)^2 q_2(t) + b_{222} q_2(t)^3 + b_1 q_1(t) + b_{11} q_1(t)^2 + b_{111} q_1(t)^3 = f_{22}\cos(\Omega_2 t) \tag{19b}$$

where f_{ij} is the amplitude of the single-harmonic functions, and $a_i, b_i, c_i, a_{ij}, b_{ij}, a_{ijk}$, and b_{ijk} are the Galerkin coefficients of the beam and cable, which are defined in the Appendix. From (19a), it is evident that some nonlinearity (quadratic and cubic) exists due to the coupled behavior between the modes of the beam

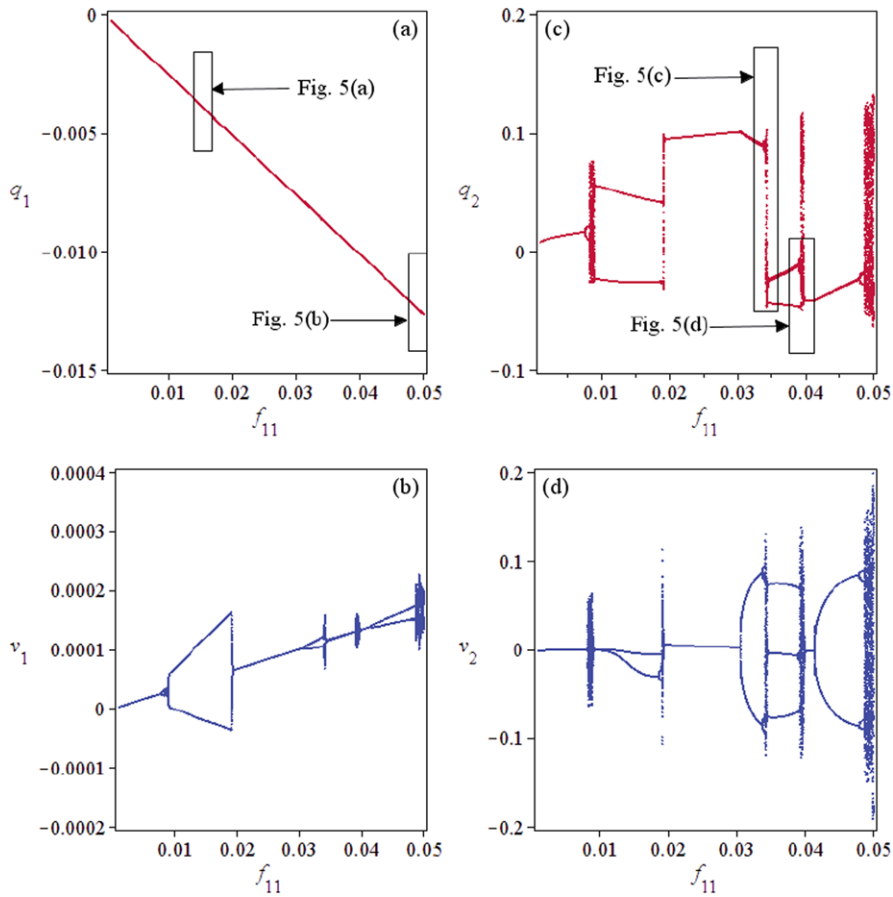

Fig. 4 Bifurcation diagrams for the sub-harmonic resonance to the beam ($\omega_1 : \Omega_1 = 1:2$) and principal resonance to the cable ($\omega_2 : \Omega_1 = 2:2$) when the excitation directly acting on the beam: (**a**) the beam's modal amplitude; (**b**) the beam's modal velocity; (**c**) the cable's modal amplitude; (**d**) the cable's modal velocity

and the cable, although the beam model is considered linearized. From (19b), it is evident that the nonlinear term is richer than the case that only considers the geometric nonlinearity in a cable.

3 Bifurcation and chaos

The bifurcation diagram is a modern technique used to analyze nonlinear systems. In a bifurcation diagram, the characteristic of the motion of a system is qualitatively changed as a parameter varies across a specific value. It reveals that a previous motion loses stability at a bifurcation point across which a new motion is originated. Thus, the bifurcation diagram provides a summary of essential dynamics and is therefore a useful tool for acquiring an overview. In order to content the 1:2 internal condition ($\omega_1 = 1.000$ and $\omega_2 = 1.978$), the cable–beam coupled system parameters are set to $\rho = 0.01$, $\chi = 0.04$, $\mu = 1000$, $\upsilon = 0.0345$, $\xi_1 = \xi_2 = 0.01$, and $\theta = \pi/3$. The truncated model equations are solved by the fourth-order Runge–Kutta algorithm with an integration step size of 0.00001 and the transient solutions are discarded.

3.1 Excitation acting on the cable

When the excitation directly acting on the cable, the set of (19a), (19b) can be simplified to four-dimensional nonlinear averaged equations in Cartesian form:

$$\dot{q}_1(t) = v_1(t) \tag{20a}$$

$$\begin{aligned}\dot{v}_1(t) = &-a_1 q_1(t) - a_{12} q_2(t) q_1(t) - a_{122} q_2(t)^2 q_1(t) \\ &- a_{11} q_1(t)^2 - a_{112} q_2(t) q_1(t)^2 \\ &- a_{111} q_1(t)^3 - \xi_1 v_1(t)\end{aligned} \tag{20b}$$

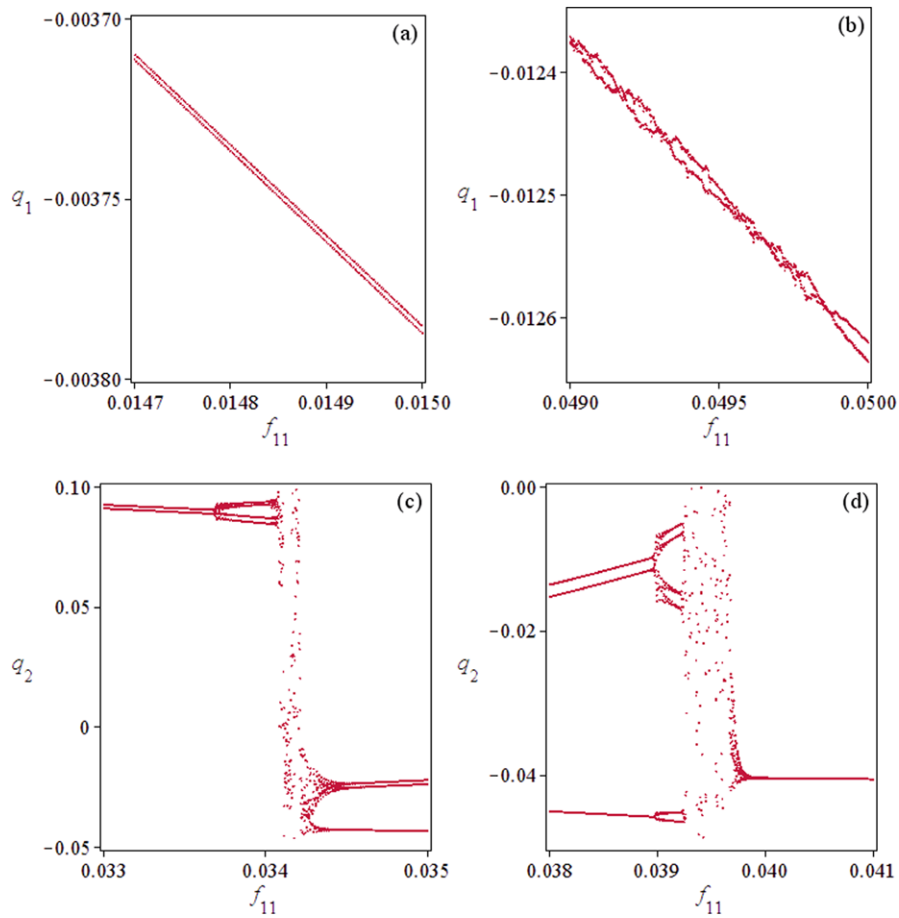

Fig. 5 Local magnification of Figs. 4(a) and 4(c)

$$\dot{q}_2(t) = v_2(t) \tag{20c}$$

$$\begin{aligned}\dot{v}_2(t) = &-b_2 q_2(t) - b_{12} q_1(t) q_2(t) + c_1 a_{12} q_1(t) q_2(t) \\ &- b_{22} q_2(t)^2 - b_{122} q_1(t) q_2(t)^2 \\ &+ c_1 a_{122} q_1(t) q_2(t)^2 - b_{222} q_2(t)^3 \\ &+ c_1 a_1 q_1(t) - b_1 q_1(t) - b_{11} q_1(t)^2 \\ &+ c_1 a_{11} q_1(t)^2 - b_{112} q_1(t)^2 q_2(t) \\ &+ c_1 a_{112} q_1(t)^2 q_2(t) - b_{111} q_1(t)^3 \\ &+ c_1 a_{111} q_1(t)^3 - c_2 v_1(t) + c_1 \xi_1 v_1(t) \\ &- \xi_2 v_2(t) + f_{22} \cos(\Omega_2 t)\end{aligned} \tag{20d}$$

From (20a)–(20d) it is evident that the term of excitation only appears in the governing equations of the cable. This indicates that the beam motion is free vibration and there is no dynamic response due to its initial displacement is zero (as seen in (18a)). Thus, in this case, there is no coupled behavior between the beam and the cable. The nonlinear responses that are caused solely by the geometric nonlinearity have been studied extensively in a lot of literatures [6, 18, 19] and, as such, we do not examine this issue.

3.2 Excitation acting on the beam

When the excitation directly acting on the beam, the set of (19a), (19b) can be simplified into the following form:

$$\dot{q}_1(t) = v_1(t) \tag{21a}$$

$$\begin{aligned}\dot{v}_1(t) = &-a_1 q_1(t) - a_{12} q_2(t) q_1(t) - a_{122} q_2(t)^2 q_1(t) \\ &- a_{11} q_1(t)^2 - a_{112} q_2(t) q_1(t)^2 - a_{111} q_1(t)^3 \\ &- \xi_1 v_1(t) + f_{11} \cos(\Omega_1 t)\end{aligned} \tag{21b}$$

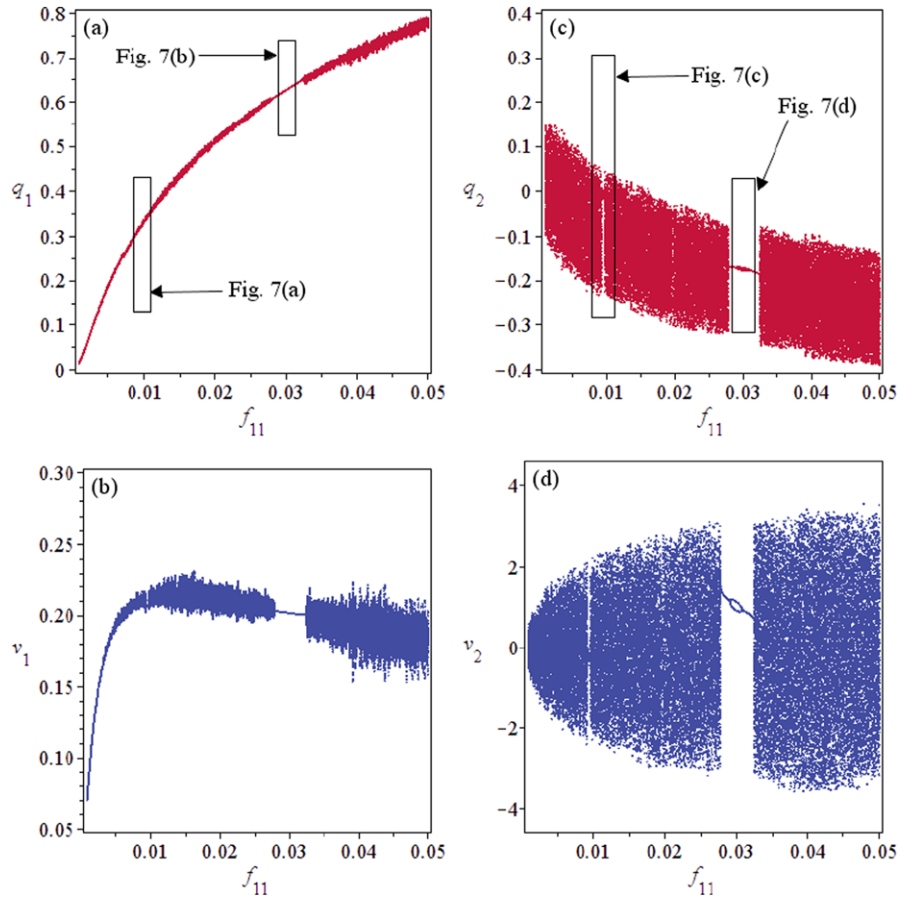

Fig. 6 Bifurcation diagrams for the primary resonance to the beam ($\omega_1 : \Omega_1 = 1:1$) and supre-harmonic resonance to the cable ($\omega_2 : \Omega_1 = 2:1$) when the excitation directly simultaneous acting on the beam and cable: (**a**) the beam's modal amplitude; (**b**) the beam's modal velocity; (**c**) the cable's modal amplitude; (**d**) the cable's modal velocity

$$\dot{q}_2(t) = v_2(t) \tag{21c}$$

$$\begin{aligned}\dot{v}_2(t) = &-b_2 q_2(t) - b_{12} q_1(t) q_2(t) + c_1 a_{12} q_1(t) q_2(t) \\ &- b_{22} q_2(t)^2 - b_{122} q_1(t) q_2(t)^2 \\ &+ c_1 a_{122} q_1(t) q_2(t)^2 - b_{222} q_2(t)^3 \\ &+ c_1 a_1 q_1(t) - b_1 q_1(t) - b_{11} q_1(t)^2 \\ &+ c_1 a_{11} q_1(t)^2 - b_{112} q_1(t)^2 q_2(t) \\ &+ c_1 a_{112} q_1(t)^2 q_2(t) - b_{111} q_1(t)^3 \\ &+ c_1 a_{111} q_1(t)^3 - c_2 v_1(t) + c_1 \xi_1 v_1(t) \\ &- \xi_2 v_2(t) - c_1 f_{11} \cos(\Omega_1 t)\end{aligned} \tag{21d}$$

From (21a)–(21d), it is evident that the terms of excitation both appear in the governing equations of the beam and cable, indicating that the nonlinear term is not only due to the cable's geometric behavior, but is also due to the coupled behavior between the beam and the cable. Therefore, under the condition of 1 : 2 internal resonant between the modes of the beam and the cable, two separate external resonance cases, $\Omega_1 = 1$ and $\Omega_1 = 2$, are analyzed: the primary and subharmonic resonance for the beam, and the corresponding auto parametric and principle parametric resonance for the cable.

Figure 2 shows the bifurcation diagrams as the forcing amplitude (f_{11}) is varied in the range $0.001 \leq f_{11} \leq 0.05$; the values of other parameters are all fixed when there is primary resonance for the beam and auto parametric resonance for the cable. As seen in Fig. 2, it can be observed that the dynamic behaviors of the beam and the cable are always consistent when they act as an overall structure. The beam and cable motions mainly exhibit chaos, and only a few periodic motion windows exist in some very small regions (as seen in Fig. 3). When the forcing amplitude (f_{11}) is small, as seen in Fig. 3(c), there are some periodic-

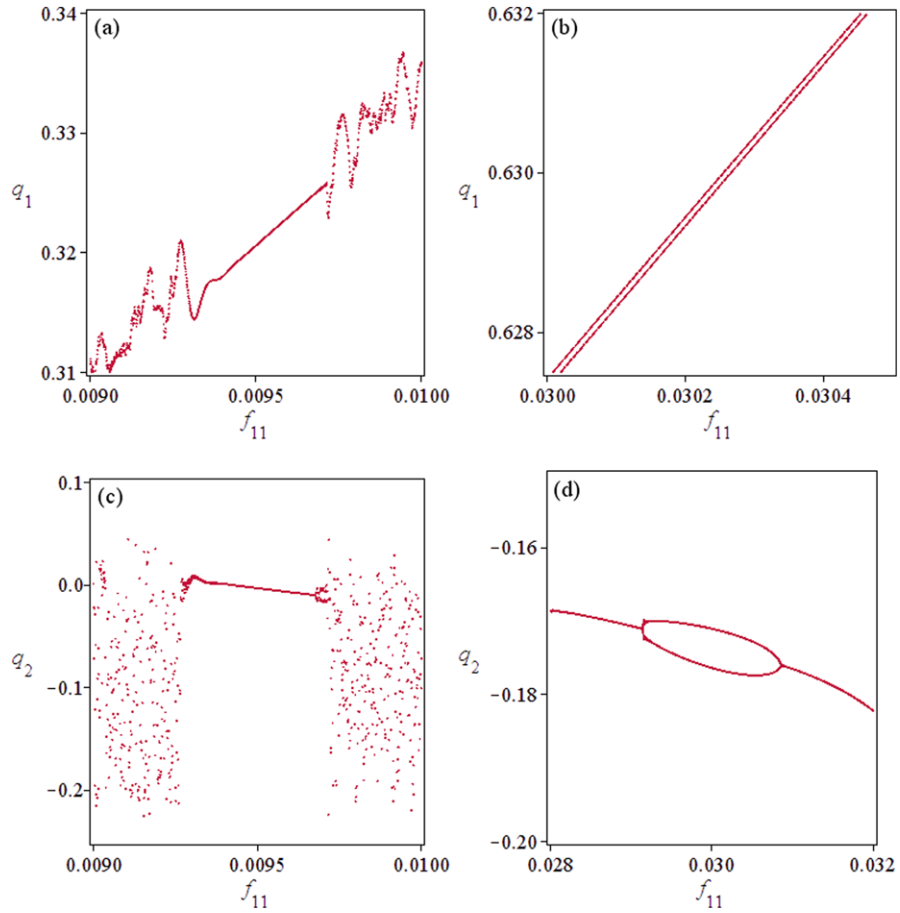

Fig. 7 Local magnification of Figs. 6(a) and 6(c)

2 motion windows for the cable. The same dynamic behaviors for the beam can be seen in Fig. 3(a). Referring to Figs. 2(a) and 2(b), although the chaotic motion of the beam becomes more obvious with the forcing amplitude (f_{11}) increasing, its response is very small compared to the cable. Moreover, as seen in Figs. 2(a) and 2(c), the modal amplitude of the beam and the cable is always along the positive direction and negative direction, respectively.

Figure 4 shows the bifurcation diagrams as the forcing amplitude (f_{11}) is varied in the range $0.001 \leq f_{11} \leq 0.05$; the values of other parameters are all fixed when there is subharmonic for the beam and principle parametric resonance for the cable. As seen in Fig. 4(a), the beam motion is almost always present in periodicity and the modal amplitude is always along the negative direction. However, due to the beam and cable act as a coupled system, the beam motion has the same characteristic as the cable, i.e., periodic-2 (Fig. 5(a)) and chaotic motions (Fig. 5(b)). Compared to Figs. 4(a) and 4(b), Figs. 4(c) and 4(d) exhibit more clearly dynamic behaviors of the cable–beam coupled system through the cable's motion. When increasing the forcing amplitude (f_{11}), the chaotic and periodic motions occur alternately, and some higher periodic motions, i.e., periodic-4 and periodic-6 can be clearly seen in Figs. 5(c) and 5(d). Compared to what seen in Fig. 2, the diversities of periodic motion become rich and the chaotic motion regions obviously decrease, indicating that the cable–beam coupled system become more stable as the resonance mechanism on the cable changes.

3.3 Excitation force acting on both the beam and the cable

In this section, the bifurcations of cable–beam coupled system are further investigated when the vertical harmonic force directly acting on both the beam and the cable. In this case, we only consider the beam and

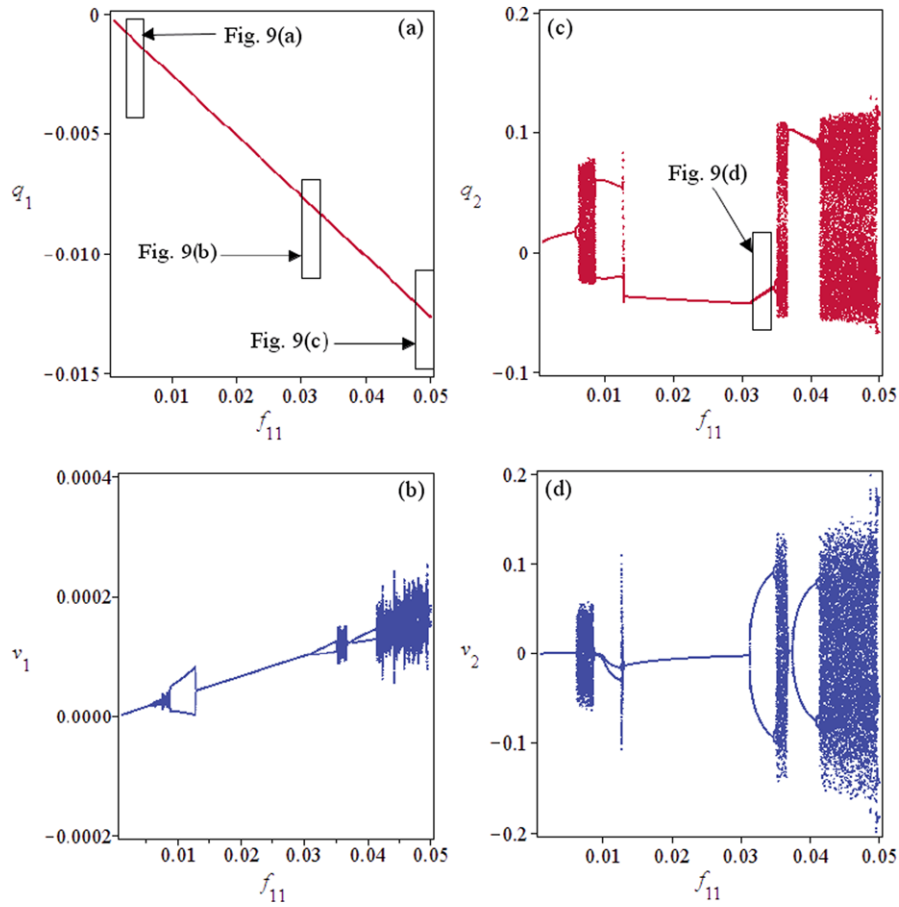

Fig. 8 Bifurcation diagrams for the sub-harmonic resonance to the beam ($\omega_1 : \Omega_1 = 1:2$) and primary resonance to the cable ($\omega_2 : \Omega_1 = 2:2$) when the excitation directly simultaneous acting on the beam and cable: (**a**) the beam's modal amplitude; (**b**) the beam's modal velocity; (**c**) the cable's modal amplitude; (**d**) the cable's modal velocity

cable in the same load environment, i.e., wind load. The forcing frequencies and amplitudes are set to Ω_1 and f_{11}. Under the condition of $1:2$ internal resonance between the modes of the beam and cable, two separate forcing frequency cases, $\Omega_1 = 1$ and $\Omega_1 = 2$, are considered. The former corresponds to the primary resonance for the beam and simultaneous superharmonic resonance for the cable. The latter corresponds to sub-harmonic resonance for the beam and simultaneous primary resonance for the cable.

Similarly as before, solutions of (19a), (19b) are obtained by using the fourth-order Runge–Kutta algorithm, with the same parameters and initial conditions employed in the foregoing. Figures 6 and 8 show the bifurcation diagrams as the forcing amplitude (f_{11}) is varied as $0.001 \leq f_{11} \leq 0.05$; the values of other parameters are all fixed for the forcing frequency $\Omega_1 = 1$ and $\Omega_1 = 2$, respectively. As seen in Figs. 6 and 8, it can be observed that the beam and cable exhibit a similar dynamic behavior to what seen in Figs. 2 and 4, respectively. However, there are some differences between them for each case since the two external resonances exist simultaneously. When the forcing frequency $\Omega_1 = 1$, due to the additional superharmonic for the cable, the periodic motion occurs in a relatively larger region and a periodic-2 motion occurs in the round of $f_{11} = 0.03$ (Figs. 7(b) and 7(d)). When the forcing frequency $\Omega_1 = 2$, due to the additional subharmonic for the beam, the diversities of periodic motion become poor (Figs. 9(a), 9(b) and 9(d)), i.e., periodic-3 and periodic-6 disappear, and the regions of chaotic motion obviously increase (Fig. 9(c)).

It is instructive to look at phase portraits and Poincare maps associated with various values of the forcing amplitude (f_{11}), which are shown in Figs. 10–13, corresponding to different dynamical behavior as discussed in the foregoing. As seen in Figs. 10 and 12, Figs. 10(c), 10(f), 12(c), and 12(f) show the chaotic motions and the others show periodic motions. Thus, one can see that the beam motion can display rich

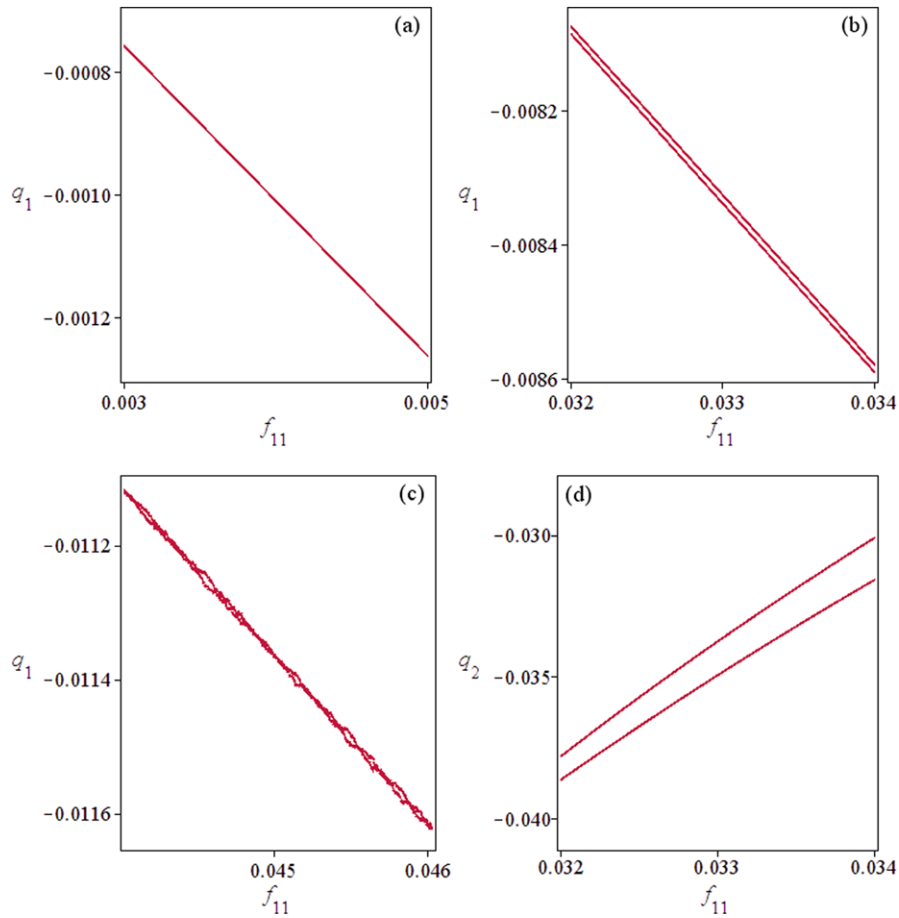

Fig. 9 Local magnification of Figs. 8(a) and 8(c)

dynamical behavior when it is coupled with the cable, even though its model is considered linearized. As seen in Figs. 11 and 13, the periodic and chaotic motions in the two cases are completely different as the resonance mechanism changing, respectively.

4 Conclusions

In this paper, the bifurcation and chaos of a cable–beam coupled system under simultaneous internal and external resonances are investigated. The combined effects of the nonlinear term due to the cable's geometry and coupled behavior (1 : 2 internal resonant) between the modes of the beam and cable are considered. The coupled nonlinear differential equations are formulated by the Hamiltonian principle. The Galerkin method is utilized to truncate the governing equations of motion to a two DOFs model. The nonlinear dynamical behaviors are numerically investigated by means of the phase portraits and the Poincare maps. Bifurcation diagrams are presented to show how the modal displacement and modal velocity changes with the forcing amplitude.

The behaviors are analyzed for three loading conditions. When the excitation directly acting on the cable, there is no dynamic response on the beam and no coupled behavior exists in the cable–beam coupled system. When the excitation directly acting on the beam, for the primary resonance to the beam and auto parametric resonance to the cable, the beam and the cable mainly exhibit chaotic motion, periodic motions only can be found in some very small regions; For the subharmonic resonance to the beam and the principal parametric resonance to the cable, the periodic motion and chaotic motion alternate, and higher periodic motion can be found. When the excitation directly acting both on the beam and cable, due to the additional su-

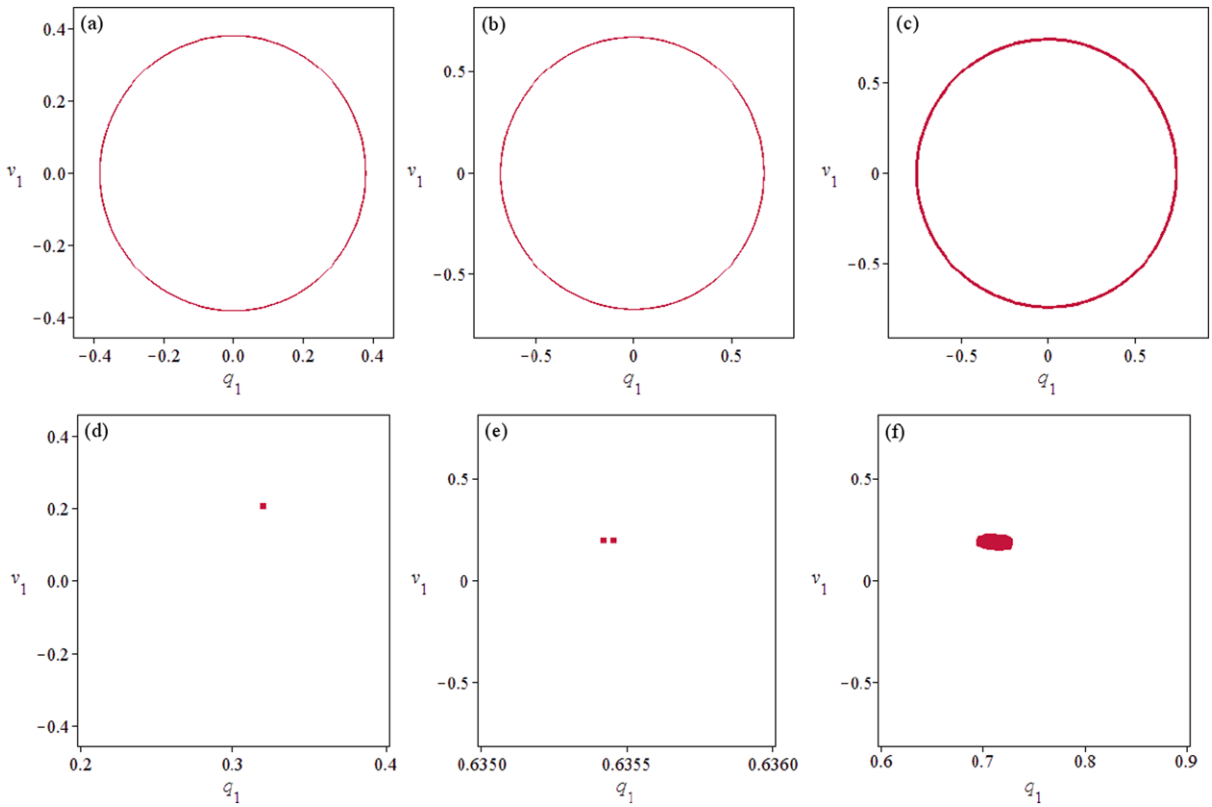

Fig. 10 Phase portraits and Poincare maps in the beam for the primary resonance to the beam ($\omega_1 : \Omega_1 = 1:1$) and supreharmonic resonance to the cable ($\omega_2 : \Omega_1 = 2:1$) when the excitation directly simultaneous acting on the beam and cable: (**a**) $f_{11} = 0.00946$; (**b**) $f_{11} = 0.0308$; (**c**) $f_{11} = 0.04$

perharmonic to the cable, the periodic motions of the cable–beam coupled system can occur in a relatively larger region. However, if the additional subharmonic to the beam exists, the diversities of periodic motion become poor. It is also found that the magnitudes of the modal displacement and velocity are equal for all cases.

Acknowledgements The present study was sponsored by National Natural Science Foundation of China (NNSFC) through Grants No. 90715031.

Appendix

First, we introduce the following integrals for defining the coefficients in (19a), (19b):

$$g_{mni} = \begin{cases} \int_0^1 y_c'(x)\varphi_n'(x)x^i & m = 3 \\ \int_0^1 \varphi_m'(x)\varphi_n'(x)x^i\,dx & m \neq 0 \end{cases}$$

$$j_{mni} = \begin{cases} \int_0^1 y_c'(x)\varphi_n(x)x^i\,dx & m = 3 \\ \int_0^1 \varphi_m'(x)\varphi_n(x)x^i\,dx & m \neq 0 \end{cases}$$

$$f_{mn} = \int_0^1 \varphi_m(x)p_n(x)\,dx$$

$$l_{mni} = \begin{cases} \int_0^1 y_c(x)\varphi_n(x)x^i\,dx & m = 3 \\ \int_0^1 \varphi_m(x)\varphi_n(x)x^i\,dx & m \neq 0 \end{cases} \tag{A.1}$$

$$r_{mni} = \begin{cases} \int_0^1 y_c''(x)\varphi_n(x)x^i\,dx & m = 3 \\ \int_0^1 \varphi_m''(x)\varphi_n(x)x^i\,dx & m \neq 0 \end{cases}$$

$$k_1 = \int_0^1 \varphi_1(x)\varphi_1(x)''''\,dx$$

where $m = 1$ or 2, $n = 1$ or 2, and $\phi_i(x)$ are the mode shapes of the beam and cable, respectively, and $y_c(x)$ is the parabola function for inclined cable.

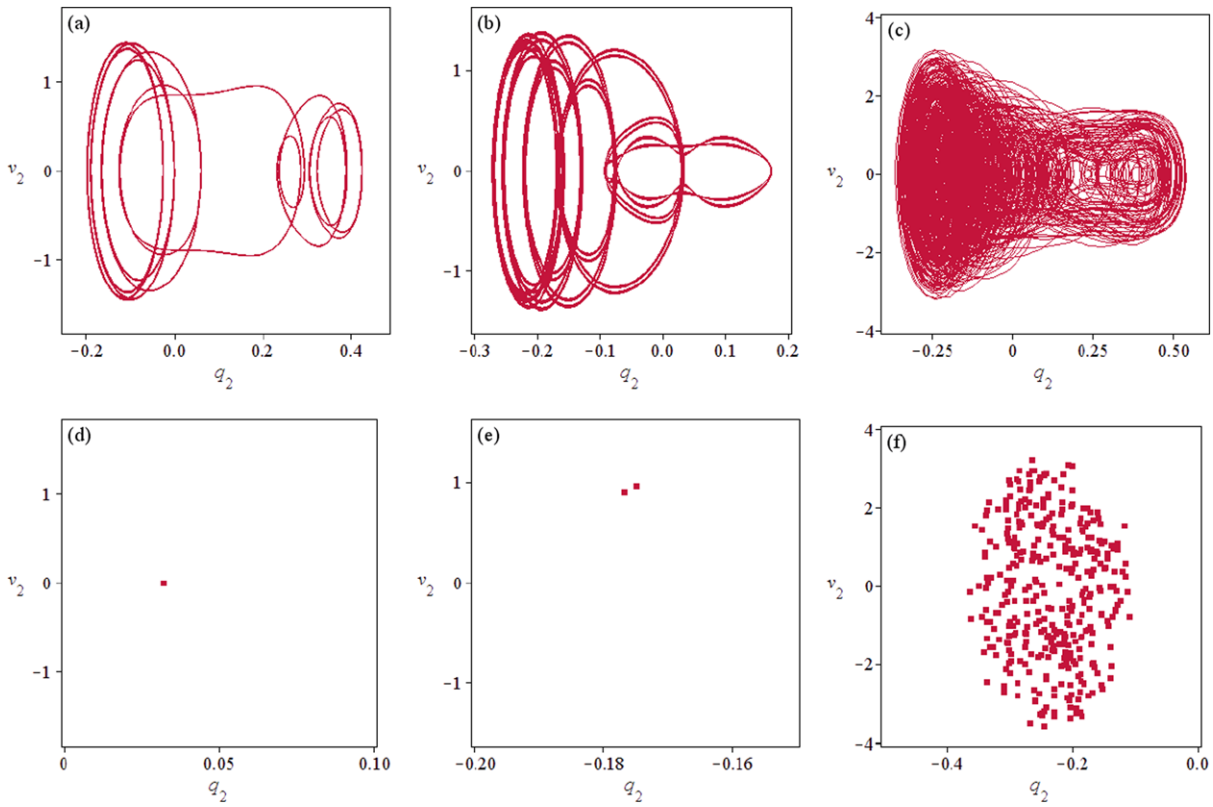

Fig. 11 Phase portraits and Poincare maps in the cable for the primary resonance to the beam ($\omega_1 : \Omega_1 = 1:1$) and supreharmonic resonance to the cable ($\omega_2 : \Omega_1 = 2:1$) when the excitation directly simultaneous acting on the beam and cable: (**a**) $f_{11} = 0.00946$; (**b**) $f_{11} = 0.0308$; (**c**) $f_{11} = 0.04$

Then the coefficients in (19a), (19b) are given as follows:

$$a_1 = \frac{k_1}{l_{110}\beta_b^4} + \frac{\rho r_{110}}{l_{110}\beta_c^2 \sin(\theta)},$$

$$a_{11} = \frac{(\nu g_{310} - \nu g_{311} - \nu j_{310})\rho\mu r_{110}\sin(\theta)}{l_{110}\beta_c^2} + \frac{\rho\mu r_{110}\varphi_1(0)\cos(\theta)}{l_{110}\beta_b^4},$$

$$a_{12} = \frac{\rho\mu r_{110} g_{320}\nu}{l_{110}\beta_c^2 \sin(\theta)},$$

$$a_{111} = \frac{\sin(\theta)^3 \rho\mu r_{110}}{\beta_c^2}\left[\frac{1}{2} + \frac{1}{l_{110}}\left(j_{111} + \frac{1}{2}g_{110} - g_{111} - j_{110} + \frac{1}{2}g_{112}\right)\right],$$

$$a_{112} = \frac{\rho\mu r_{110}\sin(\theta)}{l_{110}\beta_c^2}(g_{120} - g_{121} - j_{210}),$$

$$a_{122} = \frac{\rho\mu r_{110} g_{220}}{2 l_{110}\beta_c^2 \sin(\theta)}, \qquad f_{11} = \frac{\tilde{f}_{11}}{l_{110}},$$

$$b_1 = \frac{\sin(\theta)^2}{l_{220}\beta_c^2}\Big[(-g_{310} + g_{311} + j_{310})\mu\nu^2 r_{320} - r_{120} + r_{121} + 2j_{120} + \frac{-\mu\nu r_{320}\cos(\theta)\varphi_1(0)}{\sin(\theta)}\Big],$$

$$b_{11} = \frac{\sin(\theta)^4 \mu\nu}{l_{220}\beta_c^2}\Big(-2j_{120}g_{311} + r_{120}j_{310} - \frac{1}{2}r_{320}l_{110} + r_{121}g_{310} - r_{320}j_{111} - r_{121}j_{311} + r_{320}g_{111} + r_{320}j_{110} - r_{120}g_{310} - 2j_{120}j_{310} + r_{120}g_{311} - r_{121}j_{310} + 2j_{120}g_{310} - \frac{1}{2}r_{320}g_{110} - \frac{1}{2}r_{320}g_{112}\Big) - \frac{\cos(\theta)\varphi_1(0)}{l_{220}\beta_c^2} \times \left(-r_{120} + 2j_{120} + r_{121}\sin(\theta)^3\mu\right),$$

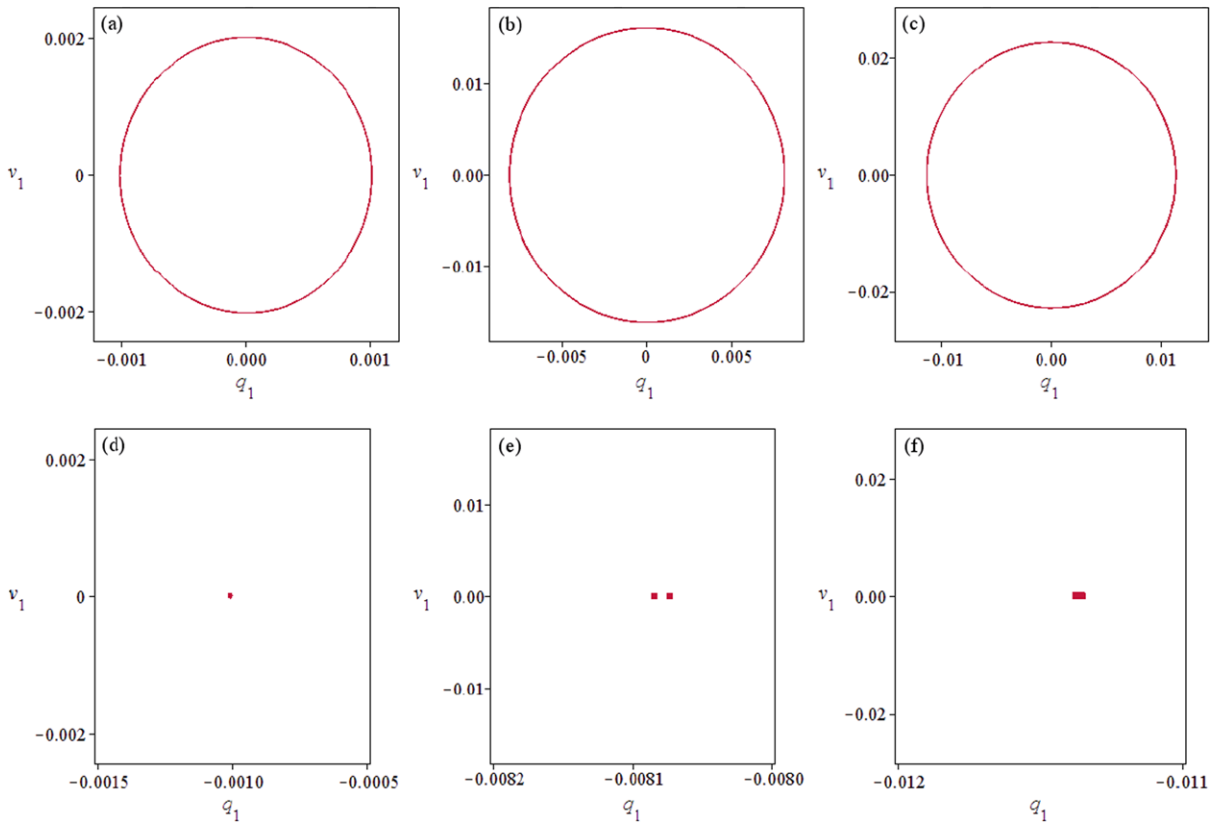

Fig. 12 Phase portraits and Poincare maps in the beam for the sub-harmonic resonance to the beam ($\omega_1 : \Omega_1 = 1:2$) and primary resonance to the cable ($\omega_2 : \Omega_1 = 2:2$) when the excitation directly simultaneous acting on the beam and cable: (**a**) $f_{11} = 0.004$; (**b**) $f_{11} = 0.032$; (**c**) $f_{11} = 0.045$

$$
\begin{aligned}
b_{111} = \frac{\sin(\theta)^6\mu}{l_{220}\beta_c^2}\Big(&-2j_{120}g_{111} + 2j_{120}j_{111} \\
&+ \frac{1}{2}r_{121}l_{110} + r_{120}g_{111} - 2j_{120}j_{110} \\
&+ r_{121}j_{111} + j_{120}g_{112} + j_{120}l_{110} \\
&- r_{121}g_{111} - r_{121}j_{110}\frac{1}{2}r_{121}g_{112} \\
&- \frac{1}{2}r_{120}g_{110} - \frac{1}{2}r_{120}g_{112} - r_{120}j_{111} \\
&- \frac{1}{2}r_{120}l_{110} + \frac{1}{2}r_{121}g_{110} + r_{120}j_{110}\Big),
\end{aligned}
\tag{A.2}
$$

$$
\begin{aligned}
b_{112} = \frac{\sin(\theta)^4\mu}{l_{220}\beta_c^2}\Big(&-\frac{1}{2}r_{220}g_{112} - \frac{1}{2}r_{220}g_{110} \\
&+ r_{121}g_{120} - r_{220}l_{110} - r_{220}l_{110} - r_{120}g_{120} \\
&- r_{121}g_{121} - r_{121}j_{210} + 2j_{120}g_{120} \\
&- 2j_{120}g_{121} - j_{120}j_{210} + r_{220}g_{111} + r_{220}j_{110} \\
&+ r_{120}g_{121} + r_{120}j_{210}\Big),
\end{aligned}
$$

$$
\begin{aligned}
b_{12} = \frac{\sin(\theta)^2\mu\nu}{l_{220}\beta_c^2}(&-r_{320}g_{120} - r_{220}g_{310} + r_{320}j_{210} \\
&+ 2j_{120}g_{320} + r_{121}g_{320} - r_{120}g_{320} + r_{220}j_{310} \\
&+ r_{320}g_{121} + r_{220}g_{311}) \\
&+ \frac{-\mu r_{220}\varphi_1(0)\sin(\theta)\cos(\theta)}{l_{220}\beta_c^2},
\end{aligned}
$$

$$
\begin{aligned}
b_{122} = \frac{\sin(\theta)^2\mu}{l_{220}\beta_c^2}\Big(&j_{120}g_{220} - \frac{1}{2}r_{120}g_{220} + r_{220}j_{210} \\
&+ \frac{1}{2}r_{121}g_{220} - r_{220}g_{120} + r_{220}g_{121}\Big),
\end{aligned}
$$

$$
\begin{aligned}
b_{122} = \frac{\sin(\theta)^2\mu}{l_{220}\beta_c^2}\Big(&j_{120}g_{220} - \frac{1}{2}r_{120}g_{220} + r_{220}j_{210} \\
&+ \frac{1}{2}r_{121}g_{220} - r_{220}g_{120} + r_{220}g_{121}\Big),
\end{aligned}
$$

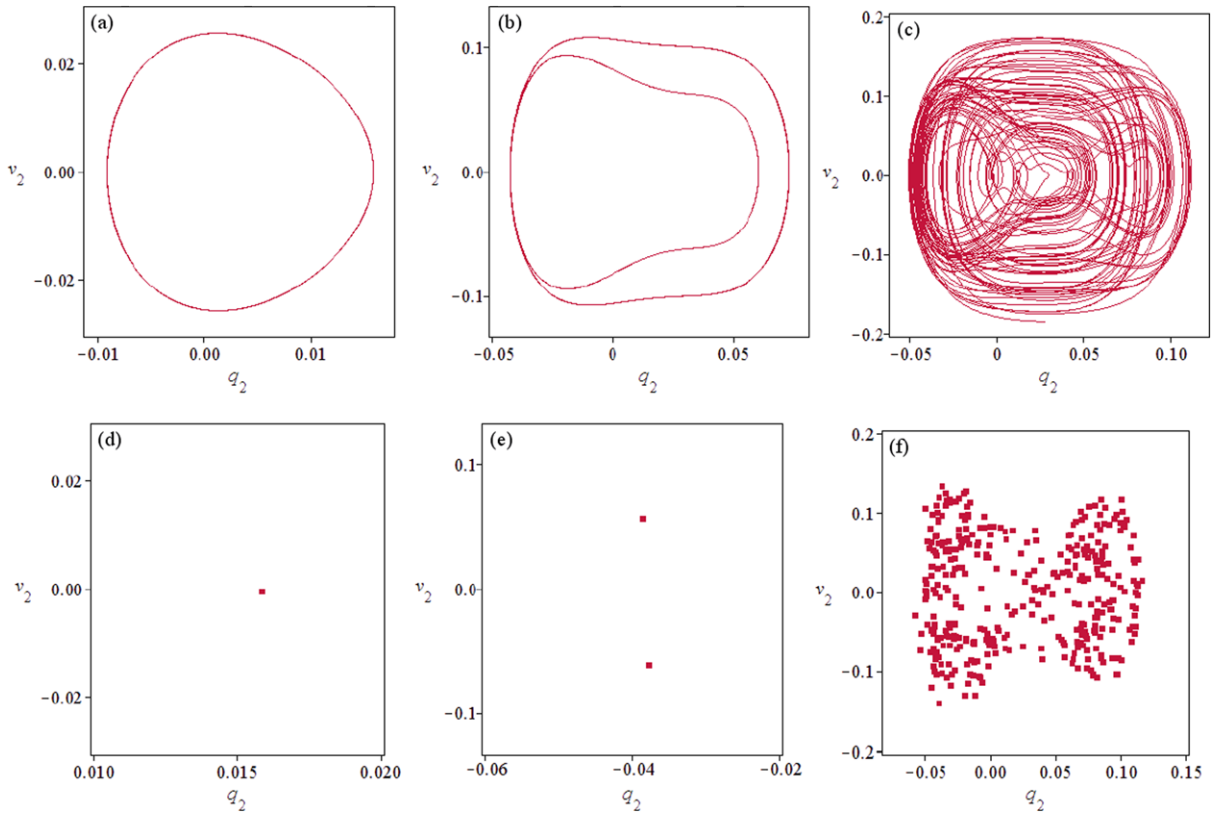

Fig. 13 Phase portraits and Poincare maps in the cable for the sub-harmonic resonance to the beam ($\omega_1 : \Omega_1 = 1:2$) and primary resonance to the cable ($\omega_2 : \Omega_1 = 2:2$) when the excitation directly simultaneous acting on the beam and cable: (**a**) $f_{11} = 0.004$; (**b**) $f_{11} = 0.032$; (**c**) $f_{11} = 0.045$

$$b_2 = \frac{-\mu v^2 r_{320} g_{320} - r_{220}}{l_{220}\beta_c^2},$$

$$b_{22} = \frac{\mu v(-r_{220} g_{320} - \frac{1}{2} r_{320} g_{220})}{l_{220}\beta_c^2},$$

$$b_{222} = \frac{\mu r_{220} g_{220}}{l_{220}\beta_c^2}\left(-\frac{1}{2}\right),$$

$$c_1 = \frac{l_{120} - l_{121}}{l_{220}} \sin(\theta)^2,$$

$$c_2 = \frac{l_{120} - l_{121}}{l_{220}} \xi_2 \sin(\theta)^2, \qquad f_{22} = \frac{\tilde{f}_{22}}{l_{220}}$$

References

1. Wang, L., Ni, Q., Huang, Y.Y.: Bifurcations and chaos in a forced cantilever system with impacts. J. Sound Vib. **296**(4–5), 1068–1078 (2006)
2. Younesian, D., Esmailzadeh, E.: Non-linear vibration of variable speed rotating viscoelastic beams. Nonlinear Dyn. **60**(1), 193–205 (2010)
3. Lenci, S., Ruzziconi, L.: Nonlinear phenomenon the single-mode dynamics of a cable-supported beam. Int. J. Bifurc. Chaos Appl. Sci. Eng. **19**(3), 923–945 (2009)
4. Wang, L.H., Zhao, Y.Y.: Nonlinear interactions and chaotic dynamics of suspended cables with three-to-one internal resonances. Int. J. Solids Struct. **43**(25–26), 7800–7819 (2006)
5. Srinil, N., Rega, G., Chucheepsakul, S.: Large amplitude three-dimensional free vibrations of inclined sagged elastic cables. Nonlinear Dyn. **33**(2), 129–154 (2003)
6. Nayfeh, A.H., Arafat, H.N., Chin, C.M., Lacarbonara, W.: Multi-mode interactions in suspended cables. J. Vib. Control **8**(3), 337–387 (2002)
7. Mamandi, A., Kargarnovin, M.H., Farsi, S.: An investigation on effects of traveling mass with variable velocity on nonlinear dynamic response of an inclined Timoshenko beam with different boundary conditions. Int. J. Mech. Sci. **52**(12), 1694–1708 (2010)
8. Kenfack, A.: Bifurcation structure of two coupled periodically driven double-well Duffing oscillators. Chaos Solitons Fractals **15**(2), 205–218 (2003)

9. Musielak, D.E., Musielak, Z.E., Benner, J.W.: Chaos and routes to chaos in coupled Duffing oscillators with multiple degrees of freedom. Chaos Solitons Fractals **24**(4), 907–922 (2005)
10. Zhang, W., Cao, D.X.: Studies on bifurcation and chaos of a string-beam coupled system with two degrees-of-freedom. Nonlinear Dyn. **45**(1–2), 131–147 (2006)
11. Zhang, W., Yao, M.: Multi-pulse orbits and chaotic dynamics in motion of parametrically excited viscoelastic moving belt. Chaos Solitons Fractals **28**(1), 42–66 (2006)
12. Brownjohn, J.M.W., Lee, J., Cheong, B.: Dynamic performance of a curved cable-stayed bridge. Eng. Struct. **21**(11), 1015–1027 (1999)
13. Caetano, E., Cunha, A., Taylor, C.A.: Investigation of dynamic cable–deck interaction in a physical model of a cable-stayed bridge. Part I: modal analysis. Earthquake Eng. Struct. Dyn. **29**(4), 481–498 (2000)
14. Au, F.T.K., Cheng, Y.S., Cheung, Y.K., Zheng, D.Y.: On the determination of natural frequencies and mode shapes of cable-stayed bridges. Appl. Math. Model. **25**(12), 1099–1115 (2001)
15. Zhou, H.B.: The experimental investigation on nonlinear dynamics of cable–beam structure. Ph.D. thesis, Hunan University (2007) (Chinese)
16. Cheng, G., Zu, J.W.: Dynamic analysis of an optical fiber coupler in telecommunications. J. Sound Vib. **268**(1), 15–31 (2003)
17. Gattulli, V., Morandini, M., Paolone, A.: A parametric analytical model for non-linear dynamics in cable-stayed beam. Earthquake Eng. Struct. Dyn. **31**(6), 1281–1300 (2002)
18. Wang, L.H., Zhao, Y.Y.: Multiple internal resonances and non-planar dynamics of shallow suspended cables to the harmonic excitations. J. Sound Vib. **319**(1–2), 1–14 (2009)
19. Kamel, M.M., Hamed, Y.S.: Nonlinear analysis of an elastic cable under harmonic excitation. Acta Mech. **214**(3–4), 315–325 (2010)